

AN ASSESSMENT OF LINEAR WRIST
MOTION DURING THE TAKING OF A
BITE OF FOOD

A Thesis
Presented to
the Graduate School of
Clemson University

In Partial Fulfillment
of the Requirements for the Degree
Master of Science
Electrical Engineering

by
Meredith Drennan
April 2010

Accepted by:
Dr. Adam W. Hoover, Committee Chair
Dr. Eric R. Muth
Dr. Richard E. Groff

ABSTRACT

Motivated by the goal of building a device capable of detecting when a user takes a bite of food, we examine whether there is a correlation between linear wrist motion and bite detection. Such a device could be used to manage weight loss by tracking eating trends over time and providing real time feedback to the user regarding eating rate or total consumption. A comprehensive analysis of tracking linear motion using low cost inertial sensors is presented. Based on this theory, we discuss the design and tracking accuracy of a prototype bite counting device. We show that tracking position using low cost, off-the-shelf sensors is impractical over any sustained period of time. However, by detecting peaks in acceleration data we are able to look for a characteristic motion during eating. We recorded data from subjects eating a meal while wearing the device. Their wrist motions were analyzed in an attempt to identify a characteristic linear motion of the wrist that corresponds to the taking of a bite of food. Our results indicate that there is too much variability in motion during eating to detect bites of food based on acceleration peaks alone.

ACKNOWLEDGEMENTS

I would like to thank my advisor, Dr. Hoover, for his patience and guidance throughout my research. I'd also like to thank my committee members, Dr. Muth and Dr. Groff for their time and effort spent reviewing this thesis. A special thanks to John Hicks for his help constructing the device. I would like to dedicate this thesis to my family for their continued support throughout my education.

TABLE OF CONTENTS

	Page
TITLE PAGE	i
ABSTRACT	ii
ACKNOWLEDGEMENTS	ii
LIST OF FIGURES	v
LIST OF TABLES	vii
1. INTRODUCTION	1
1.1 Obesity Problem	1
1.2 Current Food Intake Detection Methods	2
1.3 Tracking Motion Using Accelerometers and Gyroscopes	4
2. METHODS	5
2.1 Developing an Eating Motion Model	5
2.2 Tracking Linear Motion	7
2.3 Hardware Design	18
2.4 Unit Conversion	20
2.5 Data Smoothing	23
3. RESULTS	27
3.1 Sensor Accuracy	27
3.2 Error Propagation	29
3.3 Wrist Motion Patterns During Eating	31
3.4 Linear Wrist Motion	33
4. CONCLUSIONS	39
REFERENCES	43
APPENDIX:	46

LIST OF FIGURES

Figure	Page
2.1 Linear wrist motion prior to subject taking a bite of food.	5
2.2 Profile of wrist motion during a bite.....	6
2.3 Histogram of motion time from when wrist starts toward mouth to when food is placed in mouth.	7
2.4 Accelerometer built as a mass connected to springs.	8
2.5 Effect of gravity on measured acceleration.....	9
2.6 World and device coordinate frames.	10
2.7 Static accelerometer readings point in direction of gravity.	11
2.8 Measured acceleration is the vector sum of it's components.	11
2.9 The wrist rotates during eating.	12
2.10 Gyroscopes measure angular velocity about three orthogonal axes.	12
2.11 Tracking gravity during rotation.	13
2.12 Three rotations are required to align two coordinate systems.....	14
2.13 The DCM represents the coordinate system at time t projected onto the coordinate system at time t_0	15
2.14 Bite counter prototype.....	18
2.15 Sensor comprised of two gyroscopes and one accelerometer.	19
2.16 Sensor measurement axes.	19
2.17 Device microcontroller.	20
2.18 Data processing flowchart.....	21
2.19 Effect of gravity on the output of a 3 axis accelerometer.....	21

List of Figures (Continued)

Figure	Page
2.20 Sensitivity measurement.....	22
2.21 Acceleration profile of characteristic motion.....	24
2.22 Sampled half Gaussian.....	25
2.23 Smoothed acceleration profile of characteristic motion.	26
3.1 Experimental setup to test motion.....	27
3.2 Experiment to determine gyroscope accuracy.....	28
3.3 Gyroscope errors after 90° rotation.....	28
3.4 Translate sensor along single axis.....	29
3.5 Average accelerometer error vs distance moved.	30
3.6 Calculated gravity vector deviates from actual by an angle θ	31
3.7 Effect of angle error on position measurement.	32
3.8 Subject being recorded during a meal	33
3.9 Histogram of the time elapsed since rest at each bite detection.....	34
3.10 Complete analysis of data recorded during the taking of a bite of food by subject 1.....	36
3.11 Complete analysis of data recorded during the taking of a bite of food by subject 2.....	37
3.12 Acceleration data for five bites in which subject attempted to produce characteristic motion.	38
4.1 The effect of rate noise density and sampling frequency on position accuracy over time	40

LIST OF TABLES

Table	Page
3.1 Subject 1 bite description.....	35
3.2 Subject 2 bite description.....	35

CHAPTER 1

INTRODUCTION

This thesis considers the problem of tracking linear wrist motion during the taking of a bite of food. Previously, it has been shown that the wrist undergoes a characteristic roll motion during a bite [10]. The wrist roll is necessary to orient the hand fingers-downward to pick food up followed by fingers-sideways to place food in the mouth. Experiments have shown this motion can be used to detect bites in real time with an accuracy over 90% [20].

In this thesis we examine the linear motion made by the wrist during eating. The linear motion occurs as the wrist travels from where food is picked up to the mouth. We are interested in two questions: (1) can linear wrist motion be tracked reliably, and (2) is there a characteristic linear motion pattern that can be associated with the taking of a bite of food.

As weight gain becomes a growing problem in America we realize the need for a device capable of monitoring food intake. It is difficult for an individual to consistently monitor food intake over time. During a meal an individual may engage in a number of simultaneous activities such as talking, reading or watching television which distract from efforts meant to monitor food intake. For example, when 105 participants were asked to manually count the number of bites taken during each meal in a 24 hour period, 43 lost count or forgot entirely [15].

Limited research has developed devices capable of monitoring food intake but these are often bulky, expensive, or conspicuous. Eating occurs in a variety of environments such as homes, workplaces, restaurants and social gathering spots. For weight loss it is unlikely that a user will transport these devices to every place he or she eats due to inconvenience or embarrassment.

What is needed is a simple, low cost, non-invasive device to monitor food intake. We envision a wrist worn device that monitors consumption by detecting and recording when a bite of food is taken.

1.1 Obesity Problem

It is common knowledge that obesity and overweight are on the rise. The National Health and Nutrition Examination Survey (NHANES) [6] reports that in 2007-2008 33.8% of the adult US population was obese. This may be broken down by sex as 33.2% of men and 35.5% of women. In 2005, The World Health Organization (WHO) reported that 1.6 billion adults were obese and at least 400 million overweight based on their body mass index (BMI). Further, WHO projects that by 2015 nearly 2.3 billion adults will be overweight and 700 million obese [17].

The major reason that overweight and obesity are such a cause for concern is the associated health risks. Raised BMI is a major risk factor for diabetes, osteoarthritis, high cholesterol and certain cancers. It has also been linked to cardiovascular disease, namely heart disease and stroke, which is the leading cause of death in the world claiming 17 million lives each year [17]. In 2000 it was estimated that the cost for obesity in the US totaled more than \$117 billion [12].

Current approaches to addressing the obesity problem include diet, exercise, gastric bypass, and pharmacotherapies [25]. Although these have found success among individuals, at the societal level they have not made an impact. Over the past two decades the level of obesity among Americans has shown striking increases. One possible explanation for the lack of global success is that weight gain and loss is a long term process and the need for a long term understanding of weight gain is necessary for success [18]. It has been found that “lack of consistency in energy density” over weekly or monthly periods “rather than energy density itself” over the same time frame is most predictive of BMI [18]. By recording bite consumption over weekly, monthly, or even yearly epochs, a bite counting device hopes to foster a new area of research providing insight into the long term trends in weight gain and weight loss.

1.2 Current Food Intake Detection Methods

Recording daily consumption in a food journal is the most common method of monitoring intake. However, studies have uncovered inconsistencies that occur when individuals report their own diets [7] [11] [16] [27]. The tendency is to underreport

protien [24], fat [11], and total consumption [14] while overreporting fruit and vegetable intake [13].

PDA and web based [4] journals have also been developed to augment the individual's food journal. These methods allow the user to input their food intake and make the results available to healthcare professionals via the web. The problem with these methods is that the burden of entering information is on the user. It is difficult to get people to use them consistently over time.

One approach to monitoring food intake is to outfit the environment around the individual. Westerterp-Plantenga [28] developed a table equipped with a digital scale connected to a computer to measure consumption. Chang et al [8] also developed a dining aware table to track amount and content of food consumed. However, these methods are limited to use only when the individual eats at the table and therefore cannot provide a reliable estimate of food consumption over long periods of time.

Amft and colleagues [1] used wrist-worn sensors in conjunction with sensors on the upper arms, head, and ears, to classify an eating action taken by a person. Based on data from these sensors they sought to identify motion patterns associated with drinking, using a spoon, using cutlery, or using fingers to eat.

None of the above methods has become a widely used method of monitoring intake. The currently available methods of detecting food intake are bulky, expensive, or inconvenient. By contrast, the concept of a bite counter is simple enough that it can be implemented in a small, low cost sensor that may be worn on the wrist throughout the day with no inconvenience to the user. The key to developing a successful bite detector is realizing a simple detection algorithm that is user independent. To that effect we are examining the linear wrist motion that occurs during the taking of a bite of food.

A wrist worn bite detection device based on rotational wrist motion has been investigated previously. Results show that the roll of the wrist is a good indicator of bite detection with a sensitivity of up to 91% [10]. Preliminary studies have shown that a bite detector based on wrist roll can be employed to provide user feedback to slow eating rate [20]. We aim to further this research by developing a similar device

which detects and records bite count based on linear wrist motion.

We have developed a compact six degree of freedom inertial measurement unit (IMU) based on accelerometers and gyroscopes to measure wrist motion during eating. We address both the problem of tracking wrist motion using low cost off the shelf sensors and developing a model of characteristic motion that can be used to detect a bite.

1.3 Tracking Motion Using Accelerometers and Gyroscopes

The majority of work tracking motion with IMU sensors focuses on developing an estimation of orientation for unmanned aerial vehicle navigation. By fusing data from accelerometers and gyroscopes a reliable estimate of attitude may be produced to provide feedback to control algorithms. Inertial sensors can theoretically provide both position and orientation information based on inertial navigation system (INS) algorithms. A review of these can be found in [26].

In practice however, IMUs based on low cost MEMS sensors are not accurate enough to provide reliable position estimation over any sustained period of time. Bang and colleagues have found that after several seconds position tracking is not possible because unbounded errors introduced by sensors becomes critical [3].

IMU sensors have shown promise in gesture recognition applications. Bang et al [3] developed a pen shaped device based on accelerometers and gyroscopes to measure 3d hand writing. The 3d trajectory was projected onto a 2d plane and standard hand writing recognition algorithms were applied to the result. Cho et al. also developed a *Magic Wand* gesture input device for 3d handwriting recognition with an average success rate of 99.2% [9].



Figure 2.1 Linear wrist motion prior to subject taking a bite of food.

CHAPTER 2

METHODS

This chapter addresses both characterizing the linear wrist motion that occurs during eating and accurately tracking this motion using low cost off the shelf components in detail.

2.1 Developing an Eating Motion Model

During a meal we expect the wrist motion that will likely indicate a bite taken is the transferring of food from plate to mouth followed by a return to rest at the table. Figure 2.1 shows an example of the motion vector to be tracked.

A plot of distance moved over time of the anticipated motion would resemble the top graph in Figure 2.2 where the dashed line represents a bite detection. The graph can be characterized by two parameters, time scale and distance traversed. The motion can also be described in terms of velocity or acceleration also seen in Figure 2.2.

To determine the time scale, the data from [10] was examined. This data consists of ten videos of nine different subjects eating lunch. Each video was analyzed to determine the duration of time from when the wrist began motion toward the mouth until bite detection. A total of 322 bites were studied. Figure 2.3 shows a histogram of timing versus number of occurrences in the dataset. Over 90% of bites occurred between .5 and 2 seconds after the wrist motion toward the mouth began. This time

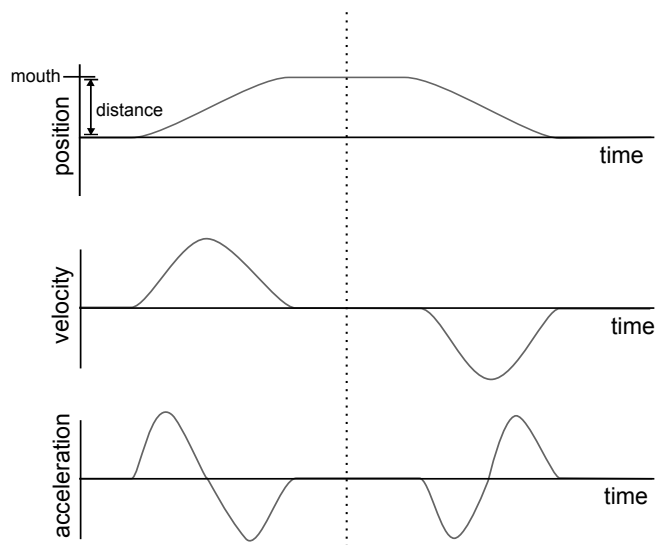


Figure 2.2 Profile of wrist motion during a bite.

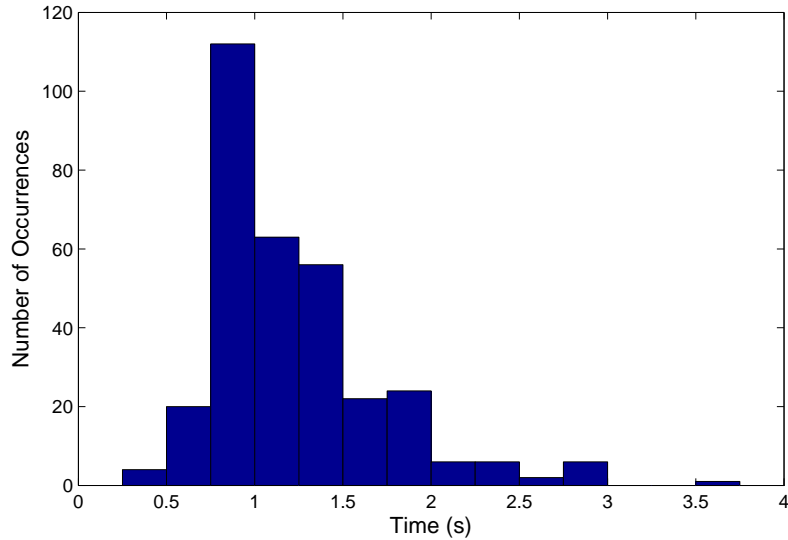


Figure 2.3 Histogram of motion time from when wrist starts toward mouth to when food is placed in mouth.

encompasses only half of the motion as the wrist will travel from mouth back to plate after the bite occurs. Therefore the bite detector must be capable of reliably tracking motion that typically lasts one to four seconds. We have hypothesized that the distance the wrist will travel from plate to mouth is between 10 and 40 cm.

2.2 Tracking Linear Motion

In order to measure wrist motion we have developed a device based on MEMS (microelectromechanical systems) linear accelerometers. An accelerometer may be thought of as a mass connected to springs, see Figure 2.4. When a force is applied to the sensor, the mass is displaced according to Hooke’s law, Equation 2.1. The force is related to acceleration through Newton’s second law of motion, Equation 2.2. Combining these two equations relates input acceleration to mass displacement as seen in Equation 2.3.

$$F = -kx \tag{2.1}$$

$$F = ma \tag{2.2}$$

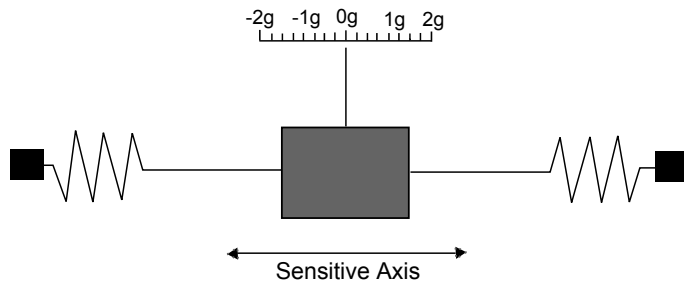


Figure 2.4 Accelerometer built as a mass connected to springs.

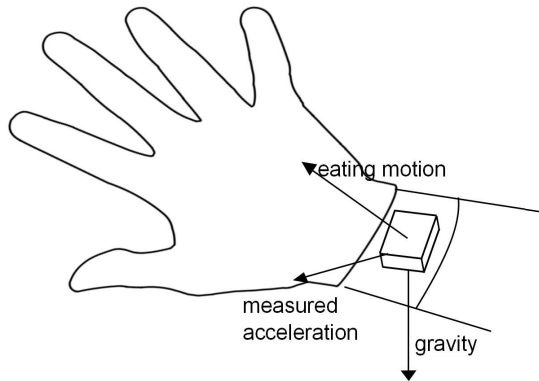


Figure 2.5 Effect of gravity on measured acceleration.

$$a = \frac{-kx}{m} \quad (2.3)$$

The force due to gravity on Earth affects the output reading of accelerometers. One can observe that if the sensitive axis of the accelerometer in Figure 2.4 is rotated clockwise 90° that the output will read $1g$.

MEMS accelerometers are designed somewhat differently than the preceding example. The LIS344alh accelerometer manufactured by STMicroelectronics [21] that we are using is capable of measuring accelerations along three orthogonal axes. It is based on capacitive strain gauges. An input acceleration causes a deviation in the capacitance of the device which is related to the sensor's output voltage via internal circuitry.

Although the mechanics of this accelerometer are different than the mass-spring example, it senses the effect of gravity in the same manner. As seen in Figure 2.5, the output of the accelerometer is the vector sum of the acceleration due to linear wrist motion and gravity.

Throughout this thesis we will adopt a convention to differentiate between the Earth's coordinate frame in which the gravity vector resides and the body frame of

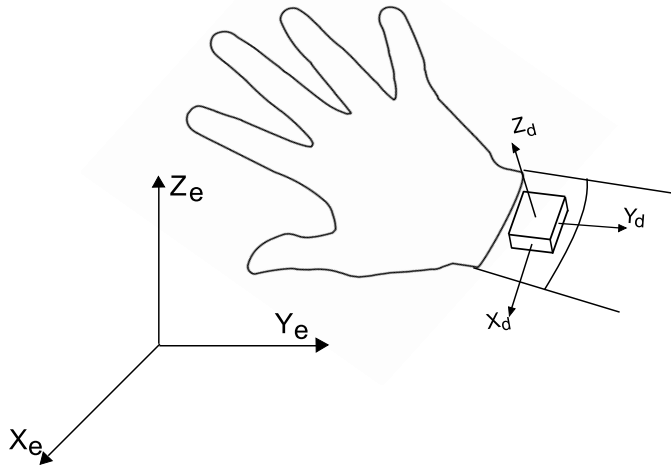


Figure 2.6 World and device coordinate frames.

the device. The two right handed coordinate systems can be seen in Figure 2.6 where the subscript d refers to the device frame and the subscript e refers to the Earth's coordinate frame.

The accelerometer we are using does not directly sense gravity but rather a deviation from freefall. This means the gravity vector is measured as $+1g$ along the Z_e axis. Therefore throughout this chapter we will denote the force due to gravity as Z_e .

In the absence of any linear motion, the accelerometer readings will point in the direction of the force due to gravity as seen in Figure 2.7.

When a linear translation is applied and the device's orientation relative to gravity does not change, linear acceleration (denoted by a lower case a), $[a_x, a_y, a_z]^T$ can be found by subtracting the accelerometer measurements experienced during the last period of rest $Z_0 = [A_{x_0}, A_{y_0}, A_{z_0}]^T$ from the measured acceleration at each timestep $[A_{x_t}, A_{y_t}, A_{z_t}]^T$ as seen in Figure 2.8.

However, Figure 2.9 shows that during eating the orientation of the device will change. In this case the system is underdetermined. The measured acceleration is known but both the direction of Z_e and the linear acceleration are unknown in

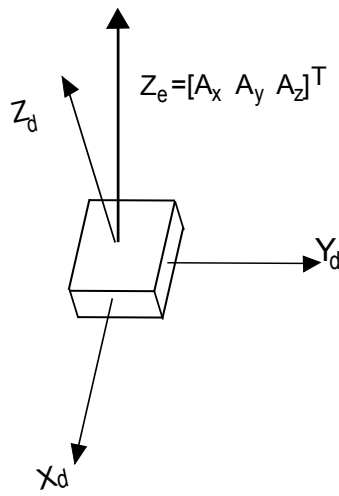


Figure 2.7 Static accelerometer readings point in direction of gravity.

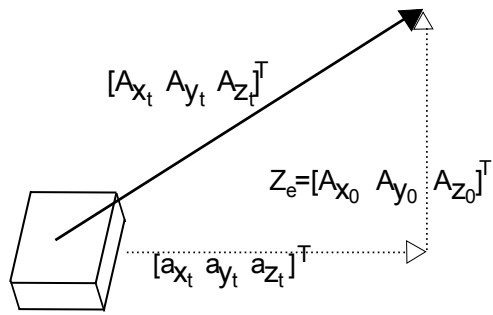


Figure 2.8 Measured acceleration is the vector sum of it's components.



Figure 2.9 The wrist rotates during eating.

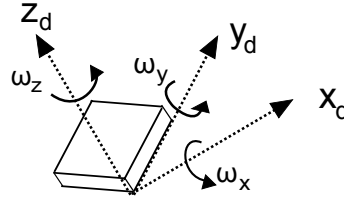


Figure 2.10 Gyroscopes measure angular velocity about three orthogonal axes.

Equation 2.4.

$$a_{linear} = A_{measured} - Z_e \quad (2.4)$$

The sensor's orientation relative to gravity must be tracked during motion in order to remove the effect of the gravity vector. To do this we incorporate rate gyroscopes into the system. The gyroscopes measure rotation about device axes as seen in Figure 2.10 where ω_x is the rotational velocity about the x axis in the device coordinate system.

Measurements from the gyroscopes update a rotation matrix which rotates the gravity vector experienced by the accelerometer during the most recent period of rest (Z_0) to its current state. See Figure 2.11.

To track the rotation from the coordinate system defined by the device axes during the last period of rest (when the effect of the gravity vector was known) to its current location we use a direction cosine matrix (DCM). The DCM is a 3x3 rotation matrix. Although there are nine elements in a 3x3 matrix, only three parameters are required to rotate one coordinate system to another in 3d space as seen in Figure

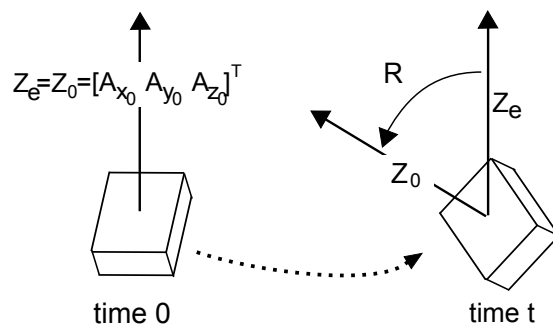


Figure 2.11 Tracking gravity during rotation.

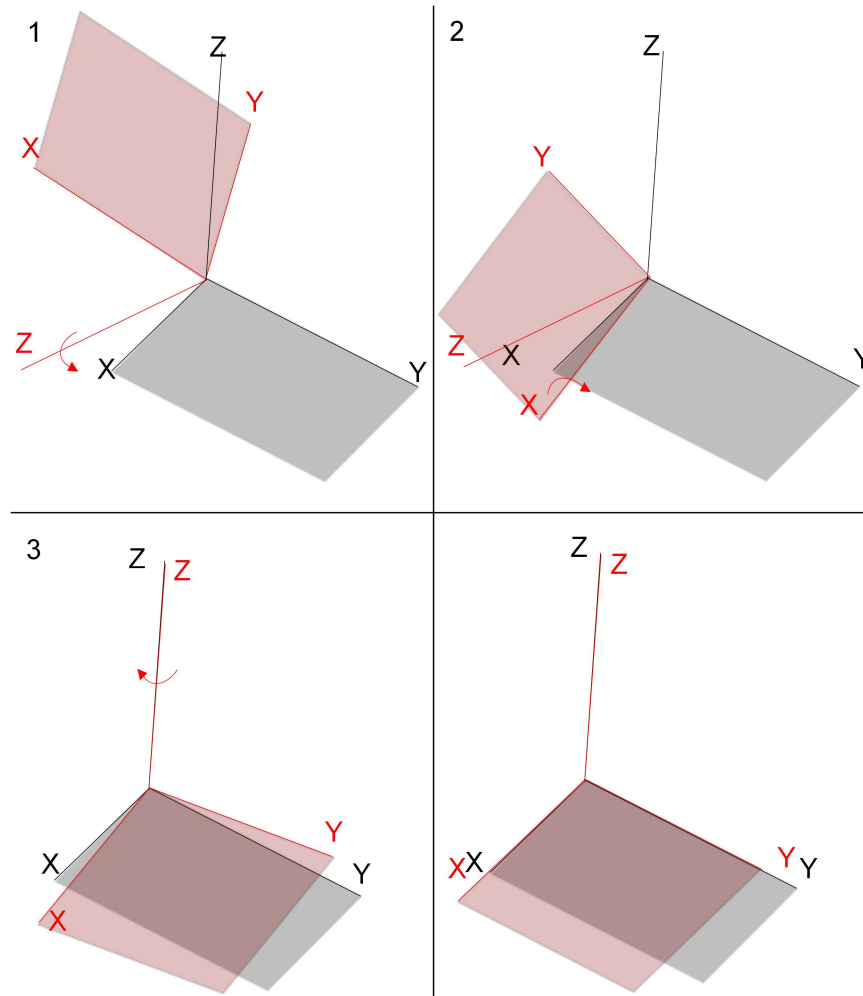


Figure 2.12 Three rotations are required to align two coordinate systems.

2.12. Therefore only three of the nine parameters are independent.

Each element ij in the DCM is the dot product of axis i at time t_0 with axis j at time t where t_0 indicates the last period of rest. See Figure 2.13. The DCM can be used to transform the vector, Z_e , as measured in the device coordinate system at time t_0 to its location at time t as seen in Equation 2.5

$$Z_0 = R_{t_0}^t Z_e \quad (2.5)$$

Equations 2.6 and 2.7 show the relationship between the DCM and the gyroscope readings. In these equations T is the inverse of the sampling frequency, ω_t is the

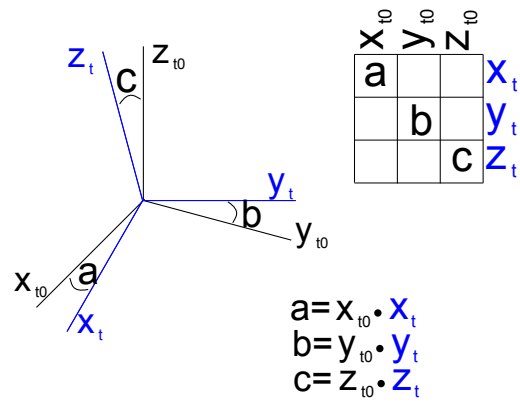


Figure 2.13 The DCM represents the coordinate system at time t projected onto the coordinate system at time t_0 .

rotational velocity of the gyroscope at time t , and δ represents the small angle rotation between time $t - 1$ and t .

$$R_{t_0}^t = R_{t_0}^{t-1} \begin{bmatrix} 1 & -\delta_z & \delta_y \\ \delta_z & 1 & -\delta_x \\ -\delta_y & \delta_x & 1 \end{bmatrix} \quad (2.6)$$

$$\delta = \omega_t T \quad (2.7)$$

Since the DCM rotates the coordinate system at time t_0 to its position at time t , the inverse can be used to compute Z_e from Z_0 . Equations 2.4 and 2.5 can be combined to yield Equation 2.8, where A is the measured acceleration, and a is the linear acceleration.

$$a_{linear} = A_{measured} - Z_e = A_{measured} - (R_{t_0}^t)^{-1} Z_0 \quad (2.8)$$

A rotation matrix by definition must be orthonormal. Each row of the matrix must be orthogonal to the other two and the magnitude of each row or column vector must be equal to 1. Over time due to numerical errors in computation, these properties will be reduced to approximations. Essentially, the vectors that define a coordinate system will begin to drift toward one another. In order to avoid the accumulation of errors, the matrix is orthonormalized after each computation as described in [19].

Let the rows of the rotation matrix R be denoted as \bar{r}_1 , \bar{r}_2 , and \bar{r}_3 respectively. First, the error is computed as the dot product between the first two rows as seen in equation 2.9. If the two vectors are orthogonal the result will be zero.

$$error = \bar{r}_1^T \bar{r}_2 \quad (2.9)$$

We distribute the error equally between the two rows and rotate the \bar{r}_1 and \bar{r}_2 rows in the opposite direction as seen in Equations 2.10 and 2.11.

$$\bar{r}_{1,orthogonal} = \bar{r}_1 - \frac{error}{2} \bar{r}_2 \quad (2.10)$$

$$\bar{r}_{2,orthogonal} = \bar{r}_2 - \frac{error}{2}\bar{r}_1 \quad (2.11)$$

After enforcing the orthogonality property on the first two rows, we compute the third row as the cross product of row 1 and row 2. See Equation 2.12.

$$\bar{r}_{3,orthogonal} = \bar{r}_{1,orthogonal} \times \bar{r}_{2,orthogonal} \quad (2.12)$$

Finally, each row vector must be normalized to a magnitude of 1. This is done by dividing each element by the magnitude of the vector as seen in Equation 2.13.

$$\bar{r}_{orthonormal} = \frac{\bar{r}_{orthogonal}}{\|\bar{r}_{orthogonal}\|} \quad (2.13)$$

The R matrix is initialized during rest. If the device is not rotating the rotation matrix reduces to the identity and the gravity vector can be subtracted as seen in Figure 2.8 to obtain linear motion.

We define a period of rest as a time when the sensor is experiencing zero velocity and assume that constant acceleration measurements over a number of samples corresponds to zero velocity. While this assumption is not valid for constant non-zero accelerations, in practice it is unlikely that a subject will maintain a constant non-zero acceleration for an extended time.

Due to noise in the system, even accelerometer measurements at rest will not be constant for any extended period of time. We therefore classify constant measurements as a period when the standard deviation of accelerometer measurements on all three axes remains below a threshold. The standard deviation calculation is performed at each timestep using equations 2.14 and 2.15. In our implementation we have set n , the number of samples in the time period, to 20. At a sample rate of 110Hz the sensor must be still for .18 seconds before a reset will occur. The threshold for rest detection was empirically determined to be .025g.

$$\bar{a} = \frac{\sum_{i=t-n+1}^t a_i}{n} \quad (2.14)$$

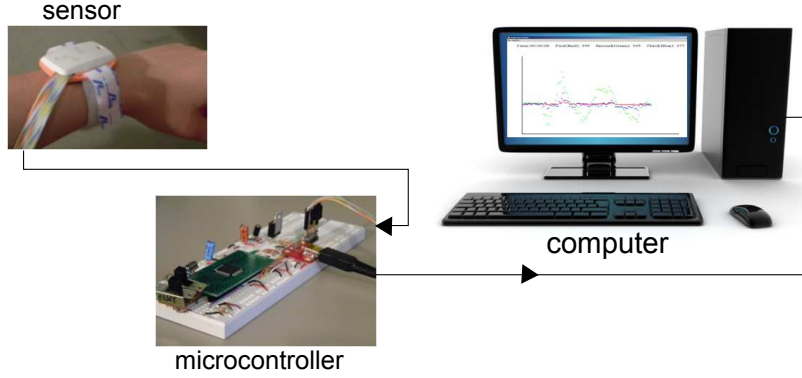


Figure 2.14 Bite counter prototype.

$$\sigma = \sqrt{\frac{\sum_{i=t-n+1}^t (a_i - \bar{a})^2}{n-1}} \quad (2.15)$$

Once the linear acceleration, a , has been computed the distance moved can be found by double integration. The Runge-Kutta method is used to numerically integrate the accelerometer data. This method uses a weighted average of the four most recent measurements to smooth the data as it integrates, see Equation 2.16.

$$V_t = V_{t-1} + \frac{T}{6}(\dot{V}_t + 2\dot{V}_{t-1} + 2\dot{V}_{t-2} + \dot{V}_{t-3}) \quad (2.16)$$

2.3 Hardware Design

We have developed a prototype wrist worn device based on the preceding theory. A high level diagram of the device can be seen in Figure 2.14. It is comprised of two major components, the sensing element and the microcontroller. The prototype device is tethered to an external computer via a USB cable which provides both power and communications with the PC.

The sensor component seen in Figure 2.15 is comprised of three chips, an accelerometer and two gyroscopes. The accelerometer is the LIS344alh chip manufactured by STMicroelectronics [21]. It is a single chip containing accelerometers on three orthogonal axes. The two gyroscopes are STMicroelectronic LPR530al [22] and



Figure 2.15 Sensor comprised of two gyroscopes and one accelerometer.

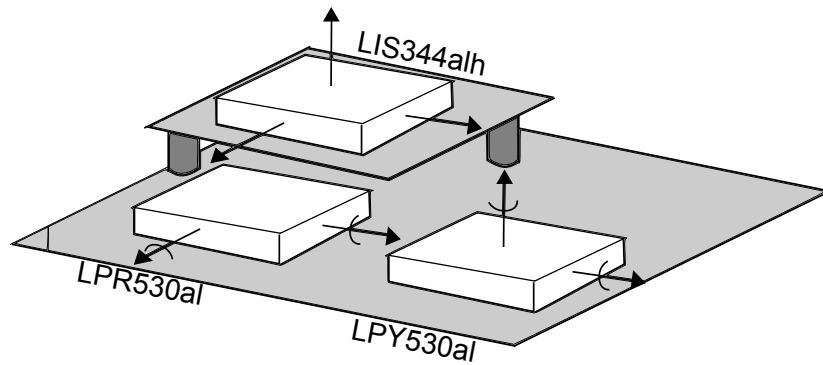


Figure 2.16 Sensor measurement axes.

LPY530al [23] gyroscopes. The chips boast the same specifications differing only in the axes of measurement. The LPR530al measures pitch and roll relative to the pins of the device while the LPY530al measures pitch and yaw relative to the device. We require gyroscope measurements on three orthogonal axes and therefore discard the redundant pitch information from the LPY530al gyro. See Figure 2.16 for an overview of measurement axes on the sensor.

The second component of the bite counter is the microcontroller which can be seen in Figure 2.17. The microcontroller, an Atmel Atmega32u4 [2], performs two tasks. First, it converts the analog measurements from the sensor to a 10 bit digital signal,

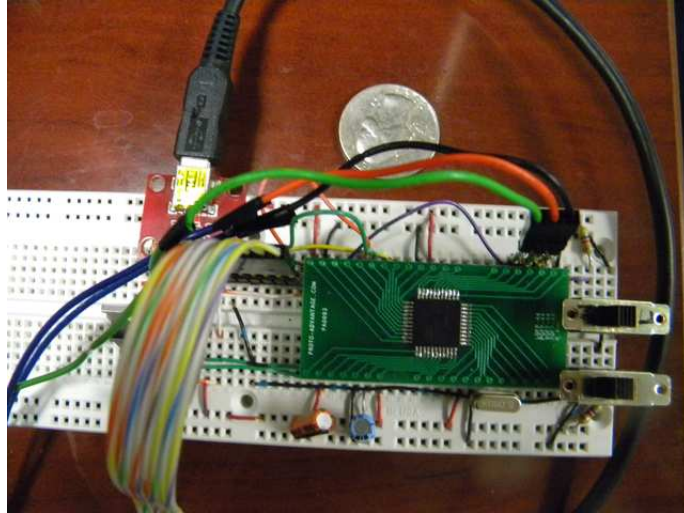


Figure 2.17 Device microcontroller.

then relays the digital measurements to the PC via a USB cable. Microcontroller firmware was developed based on Dean Camera's lightweight USB framework for AVRs (LUFA) [5].

Data collection, processing, and display is performed in real time by the computer in the C programming language. An overview of the program flow can be seen in Figure 2.18.

2.4 Unit Conversion

To convert raw acceleration measurements from volts to units of gravity see Equation 2.17. The zero G level and the sensitivity of the accelerometer are constants determined in a calibration phase. The effect of applying this equation is to first remove a DC offset from the signal then scale the output amplitude appropriately.

$$A(g) = \frac{A(v) - zeroG(v)}{Sensitivity(\frac{v}{g})} \quad (2.17)$$

At rest the accelerometer senses a static 1g acceleration distributed across its three axes due to the Earth's gravity. The output of an axis perpendicular to gravity is 0g. When an axis is parallel to gravity the magnitude of the output is 1g, see Figure 2.19. In order to calibrate the zero G level of the accelerometer, each axis was held perpendicular to gravity and the zero G output was recorded.

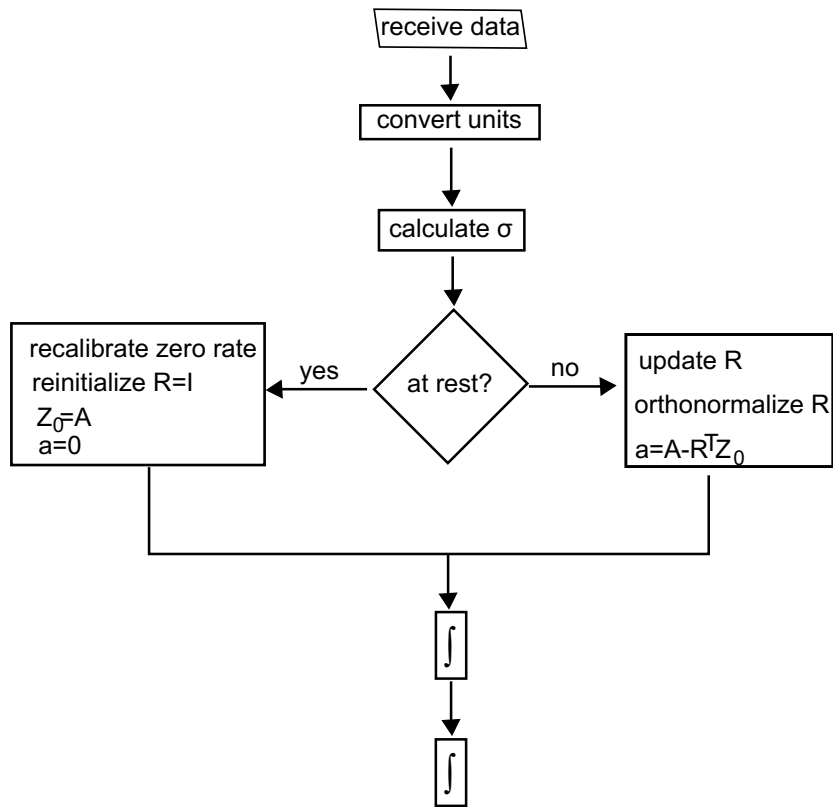


Figure 2.18 Data processing flowchart.

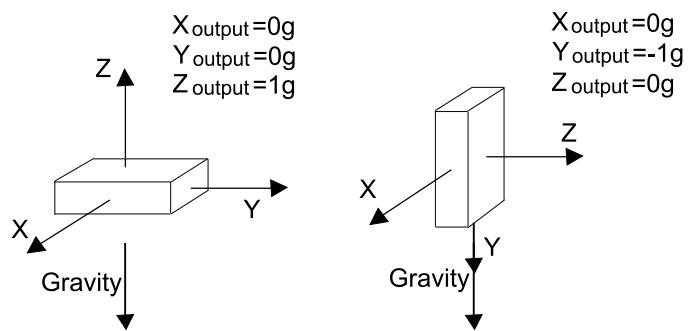


Figure 2.19 Effect of gravity on the output of a 3 axis accelerometer.

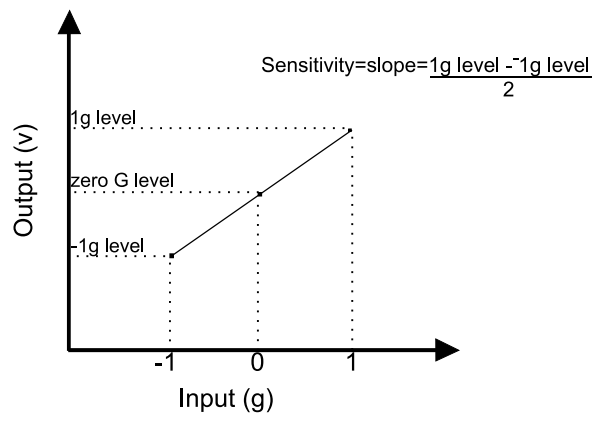


Figure 2.20 Sensitivity measurement.

The sensitivity of an accelerometer describes the change in output voltage given a 1g change in input. This value can therefore be interpreted as the slope of the line generated in Figure 2.20. The sensitivity of each axis was calibrated prior to data recording by holding the accelerometer axis still at 1g (parallel to gravity), then at -1g and finding the slope of the resultant line.

In our design, the raw measurement has been sampled by an A/D converter and must be converted to volts before applying equation 2.17.

To convert raw gyroscope measurements from volts to degrees per second Equation 2.18 is used. The zero rate level is defined in the datasheet of the LPR530al rate gyroscope as 1.23v. In practice however, the zero rate of the gyroscopes drift with time and temperature. We therefore initialize the zero rate to the average of the first 20 samples and recalibrate during periods of rest. This method assumes that the wrist is at rest when the system starts recording data. If this assumption is not upheld the data output will not be meaningful until the next registered period of rest when the gyroscope recalibrates.

$$\omega(\circ/s) = \frac{\omega(v) - ZeroRateLevel(v)}{Sensitivity(\frac{v}{\circ/s})} \quad (2.18)$$

The sensitivity of the gyroscope is listed as $3.33 \frac{mV}{\circ/s}$. This value is used to convert gyroscope measurements to degrees per second.

2.5 Data Smoothing

Using the device prototype, we recorded what we expect to be the characteristic bite motion. To do this, the device was placed on a subject's wrist. Measurements were recorded as the subject moved her wrist from table toward mouth. The subject paused briefly at the mouth and then returned her wrist to the table. The resultant acceleration data can be seen in Figure 2.21.

The output of the sensor is very noisy. In order to reduce the effects of noise, a half Gaussian smoothing filter is applied to the data. The formula for a Gaussian distribution is shown in Equation 2.19. Creating half Gaussian weights was done by sampling the continuous Gaussian function shown in Figure 2.22 where σ , the

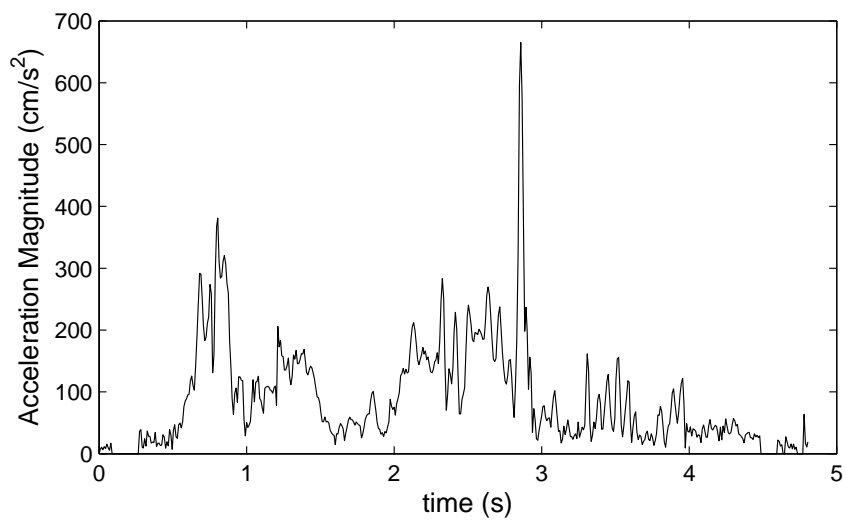


Figure 2.21 Acceleration profile of characteristic motion.

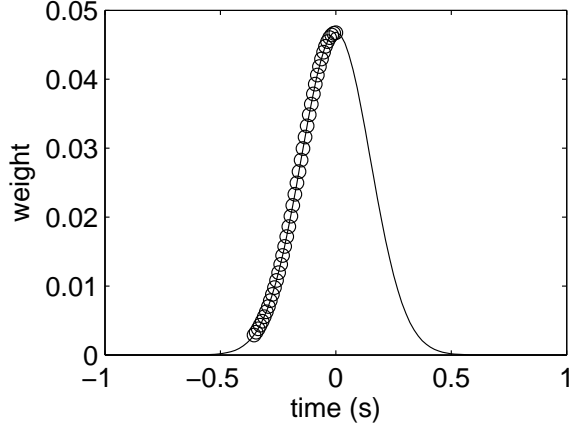


Figure 2.22 Sampled half Gaussian.

standard deviation is set to 0.15 seconds and the number of samples, N , is 40. At each sample time the smoothed data point, a_s , is computed as the sum of the past N samples multiplied by their weight as seen in Equation 2.20 and 2.21.

$$G(x) = \frac{1}{\sqrt{2\pi\sigma^2}} e^{-\frac{(x-\mu)^2}{2\sigma^2}} \quad (2.19)$$

$$a_s(t) = \sum_{i=-N}^0 w_i a_{t+i} \quad (2.20)$$

$$w_i = \frac{e^{-i^2/(2\sigma^2)}}{\sum_{j=-N}^0 e^{-j^2/(2\sigma^2)}} \quad (2.21)$$

The result of smoothing the characteristic acceleration data is seen in Figure 2.23. We expect to see two acceleration spikes each time the wrist makes a fluid motion. The first corresponds to an acceleration as motion begins, and the second, deceleration as motion ends. In Figure 2.23 peaks 1 and 2 represent the wrist motion toward the mouth, followed by a brief pause as the bite occurs and then peaks 3 and 4 indicate motion back toward the table. It is interesting to note that peaks 2 and 3 are smaller than 1 and 4. This indicates that the wearer naturally exercised more caution in motion occurring close to the mouth than the table. Another interesting feature is the spike at the end of peak 4. This spike indicates the sharp deceleration

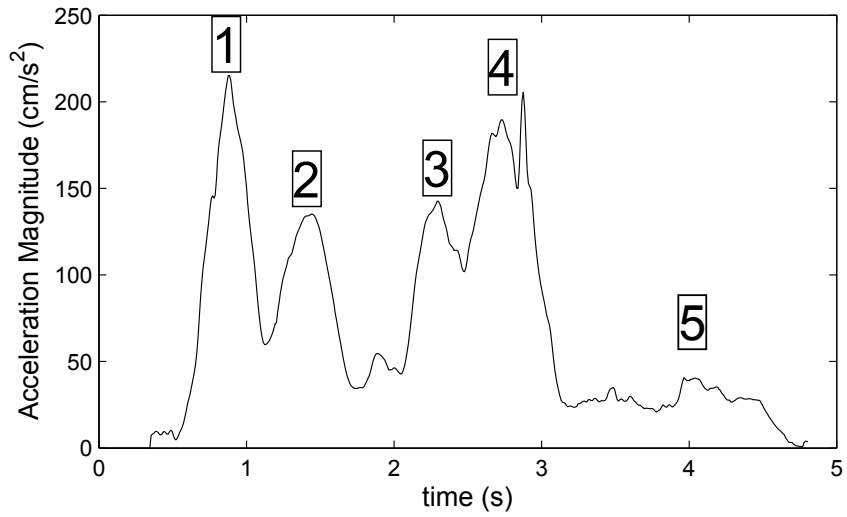


Figure 2.23 Smoothed acceleration profile of characteristic motion.

when the wrist hit the table. Finally, there is a higher noise level after the bite occurs than before indicated in Figure 2.23 by a 5. The difference in noise amplitude can be attributed to the errors that accumulate in tracking the Z_e vector over time.



Figure 3.1 Experimental setup to test motion.

CHAPTER 3

RESULTS

In this chapter we discuss the ability of our device to track motion during eating. We then investigate linear motion results from a number of recordings where users were asked to wear the device during a meal.

3.1 Sensor Accuracy

To evaluate the accuracy of the device in tracking motion, we have taken a bottom up approach. First we conducted simple experiments to evaluate the accuracy of the individual components rather than the entire sensor. Then we discuss how these errors propagate through the system.

The first test examines the accuracy of the gyroscope. To simplify the problem we applied rotation along a single axis of the gyroscope. The sensor was mounted to a wooden block such that the axis of measurement was perpendicular to a level surface as seen in Figure 3.1. The block, placed along a straight edge, was rotated 90° about the measurement axis, Figure 3.2. The results of the experiment can be seen in Figure 3.3. It is clear from these results that we can expect the gyroscope to be accurate to within two degrees.

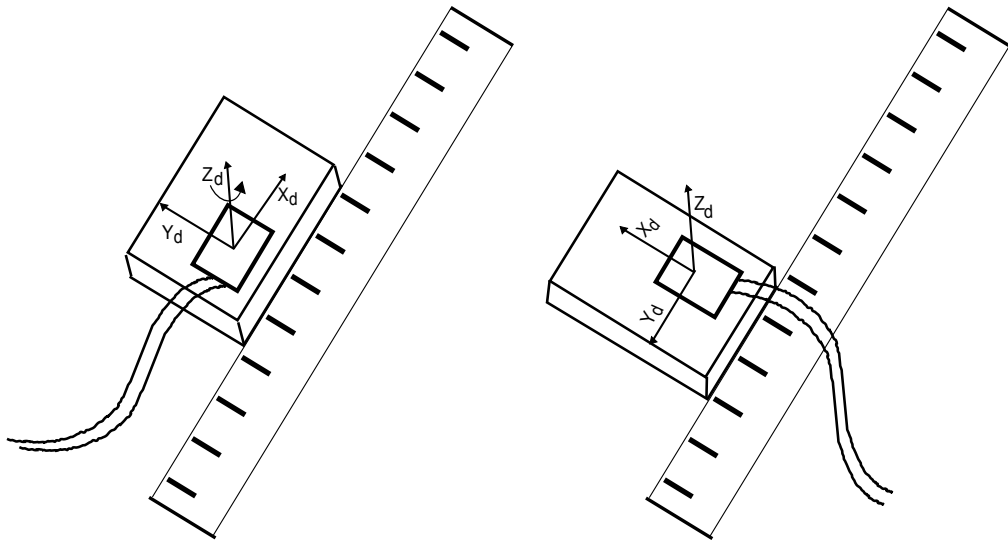


Figure 3.2 Experiment to determine gyroscope accuracy.

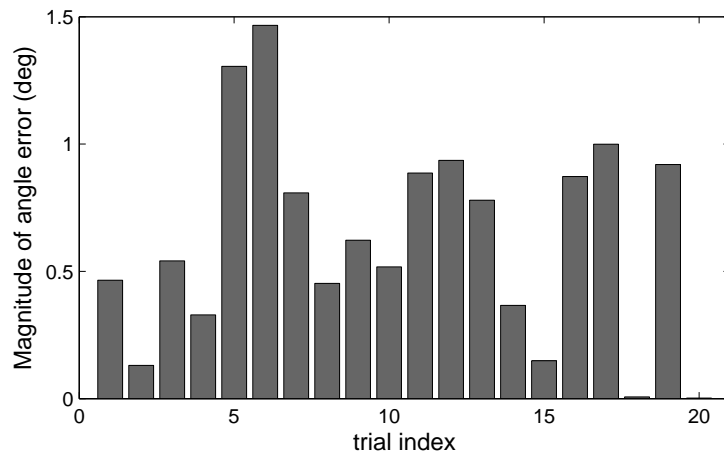


Figure 3.3 Gyroscope errors after 90° rotation.

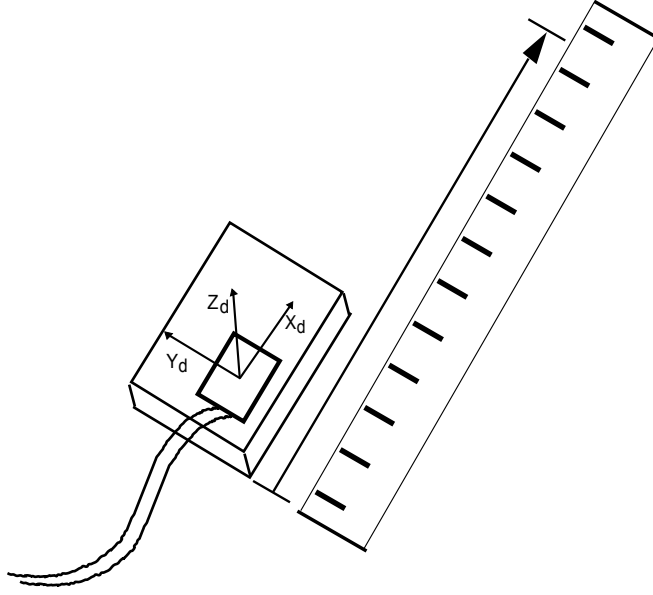


Figure 3.4 Translate sensor along single axis.

The next experiment addresses the accuracy of the accelerometer. Again we isolated the measurements to a single axis of the device, see Figure 3.4. In order to alleviate the effect of gravity from accelerometer measurements, the gravity vector Z_e , was calculated as the average of the first 20 samples and subtracted from the measurement at each timestep. The device was translated along a level surface between 10 and 40 centimeters at increments of 5 centimeters. Figure 3.5 indicates the accelerometer can track a translation on the order of 10 to 40 cm to within a few centimeters over a short time interval.

3.2 Error Propagation

Figure 3.5 shows results for a unique situation in which no rotation is applied. In our system we expect the device to rotate during eating so we now examine the effect rotation tracking errors have on linear motion tracking.

Gyroscopes are used to track the rotation of the device relative to the gravity vector. To determine how accurate the gyroscopes must be in order to successfully track position we examine the effect of a miscalculation of the gravity vector. If the calculated Z_e vector deviates from the true gravity vector by an angle θ as seen in

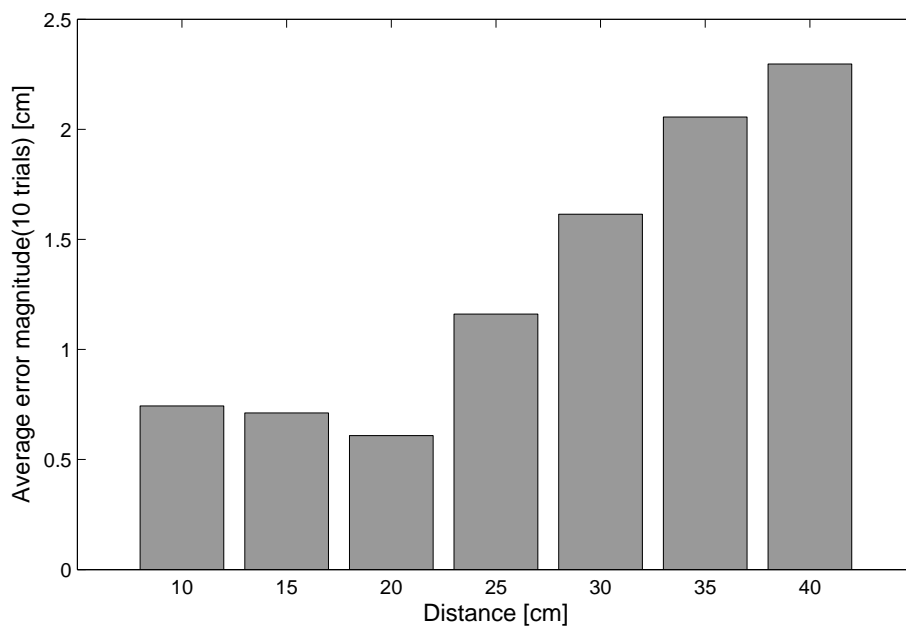


Figure 3.5 Average accelerometer error vs distance moved.

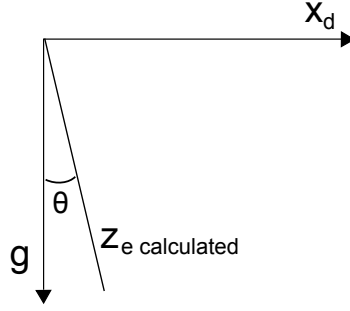


Figure 3.6 Calculated gravity vector deviates from actual by an angle θ .

Figure 3.6 the acceleration readings measure $\sin \theta g$, where g is a unit of gravity or $9.8 \frac{m}{s^2}$.

Double integration of the constant acceleration offset over time yields position errors seen in Equation 3.1.

$$Error = \frac{1}{2} \sin \theta t^2 \quad (3.1)$$

A plot of accumulated errors over a 1.5 second time interval can be seen in Figure 3.7. A miscalculation of Z_e by even one degree will result in an error in position of almost 20cm after 1.5 seconds. Our results from evaluating the gyroscope accuracy show that a deviation in angle measurement of up to two degrees can be expected. Since the anticipated position errors are on the same order of magnitude of the distance to be tracked we draw the conclusion that tracking distance with our sensors is not practical over a several second time frame.

Although gyroscope measurements may result in unbounded position errors over time we believe that by examining spikes in the acceleration data during short time intervals after rest we can still detect a user taking bites of food.

3.3 Wrist Motion Patterns During Eating

Testing this theory required gathering subjects to be recorded during meals. We recorded data from six subjects eating ten meals wearing the device. Two subjects used their hands, two used a spoon, and six used forks. The device relayed raw gyroscope and accelerometer data in real time to an on site computer via the USB

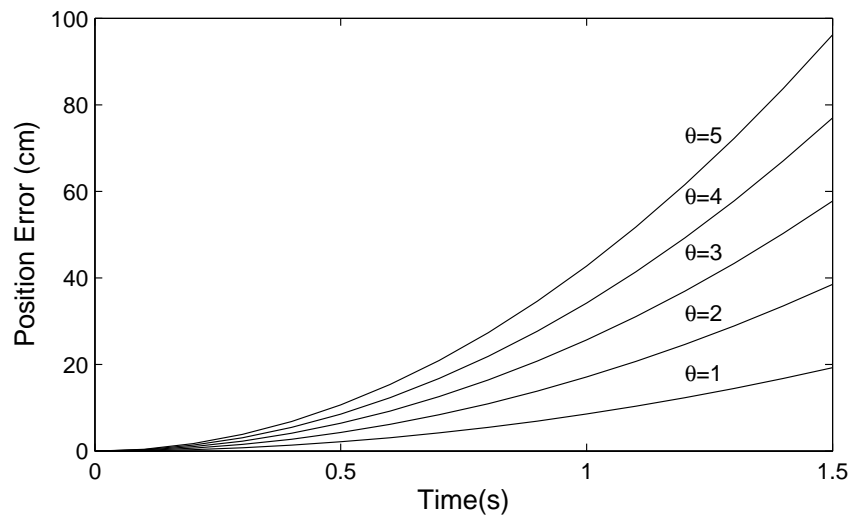


Figure 3.7 Effect of angle error on position measurement.



Figure 3.8 Subject being recorded during a meal

cable. The subjects were also video recorded in order to generate a ground truth bite detection and discover the source of any data anomalies. See Figure 3.8 for an example.

A restricting element to our study of the meal recordings is the length of time the wrist has been in motion prior to the taking of a bite of food. Motion lasting much longer than several seconds will not be discernible from the unbounded errors that propagate over time. We would like to examine only bites that occur within three seconds of a rest detection in order to ensure the data is reliable. Figure 3.9 shows a histogram of the time between the last period of rest and bite detection for the ten recordings. From this plot it is clear that the majority of bites consumed do not meet this assumption. Only 34 of the 177 bites or 19.2% occur within three seconds following a rest.

3.4 Linear Wrist Motion

Figure 3.10 shows an example of acceleration data and corresponding video frames for a bite that occurs 0.9 seconds after a period of rest. Table 3.1 is a description of the key points in Figure 3.10. In this sequence the subject begins the bite similar to what we expect with two spikes prior to bite detection indicating a fluid motion toward the

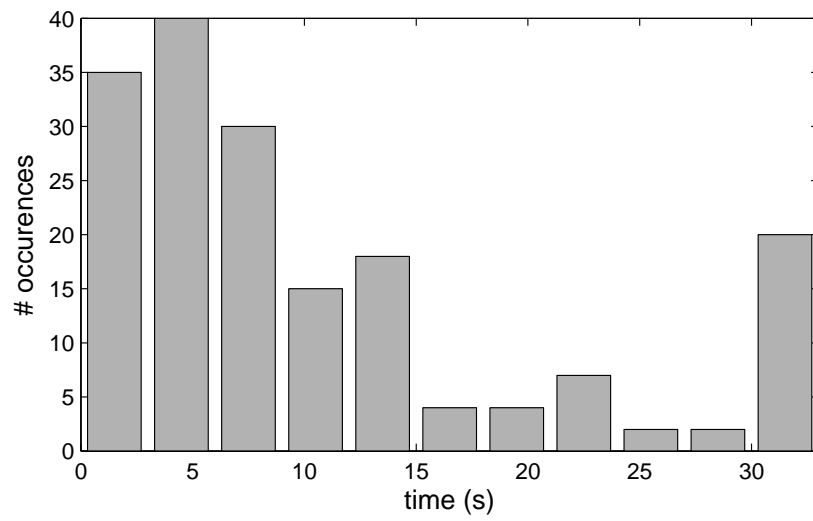


Figure 3.9 Histogram of the time elapsed since rest at each bite detection.

	Description of Action
1	wrist at rest
2	acceleration toward mouth
3	deceleration near mouth
4	bite detection
5	wrist accelerates away from mouth
6	deceleration
7	acceleration toward table
8	deceleration near table
9	wrist rests

Table 3.1 Subject 1 bite description

	Description of Action
1	wrist at rest
2	wrist begins acceleration toward mouth
3	deceleration near mouth
4	bite detection
5	wrist jerks as fork is pulled from mouth
6	acceleration away from mouth
7	deceleration as wrist nears table
8	hand reaches table
9	rest detection

Table 3.2 Subject 2 bite description

mouth followed by a bite. The motion after the bite however differs from the expected pattern. In this sequence the subject does not make a continuous motion toward the table but rather pauses briefly before reaching the table causing four spikes instead of two as he returns his wrist to the table.

A second example can be seen in Figure 3.11 and Table 3.2. This bite occurred 2.1 seconds after a rest period. At point of interest 5 in this sequence a single large spike can be seen. We saw this often when a person was eating solid foods off a fork; a spike occurs shortly after bite detection due to the motion of the wrist jerking the fork away from the mouth as he or she bites the food.

Of the 34 trackable bites none followed the expected motion pattern in Figure 2.23. Bites taken with a fork often resembled Figure 3.11 with a large spike occurring near bite detection due to pulling the fork away from the mouth. Often the individual did

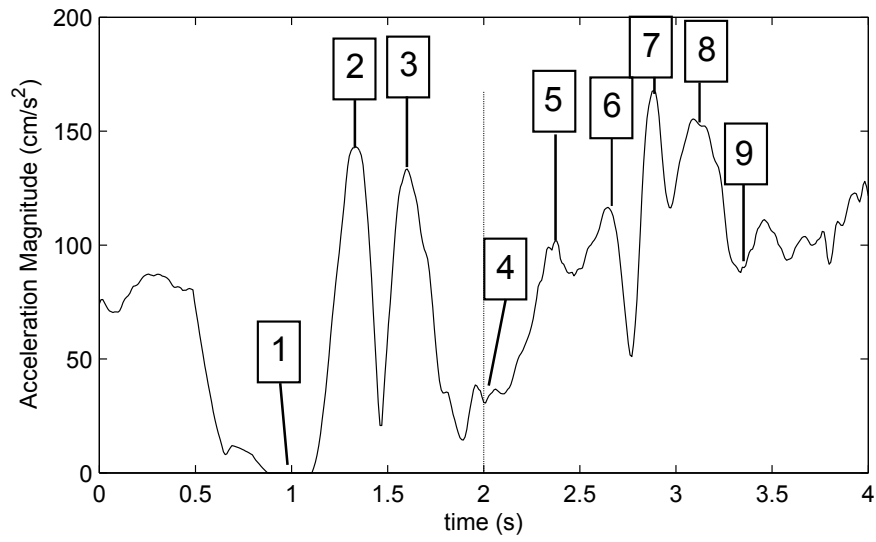


Figure 3.10 Complete analysis of data recorded during the taking of a bite of food by subject 1.

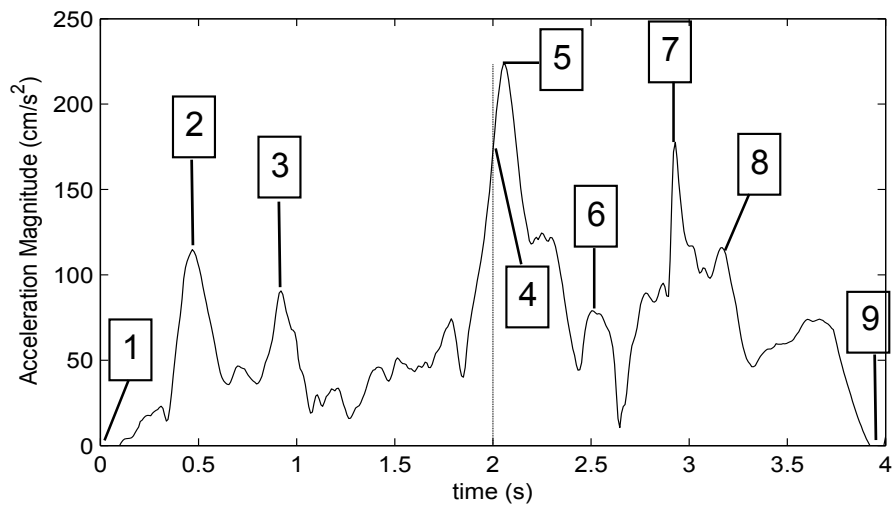


Figure 3.11 Complete analysis of data recorded during the taking of a bite of food by subject 2.

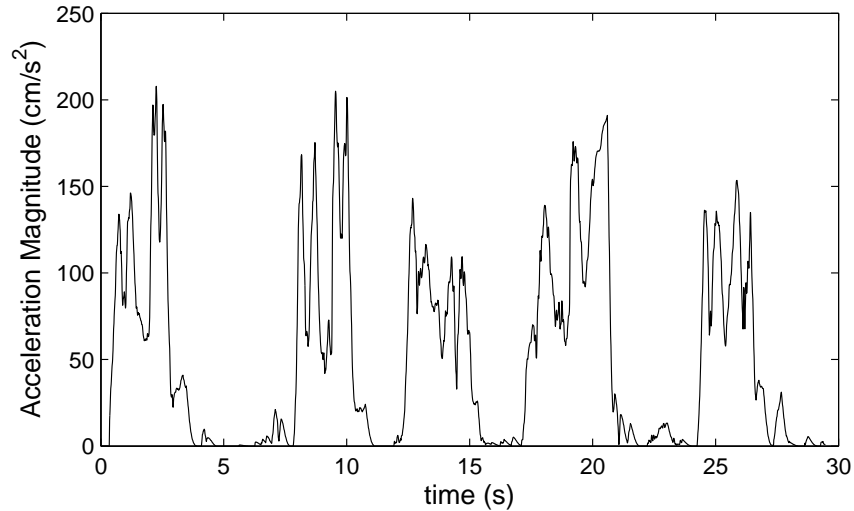


Figure 3.12 Acceleration data for five bites in which subject attempted to produce characteristic motion.

not make a fluid motion before or after the bite detection resulting in profiles such as Figure 3.10. Occasionally the subject would pause at the mouth long enough for rest detection to occur causing the peaks as the individual motioned toward the mouth to be separated from the motion away from the mouth. During some bites the user did not move deliberately enough to produce two distinct peaks corresponding to a single motion but rather the acceleration appeared as a single peak after smoothing.

These results lead us to question whether the hypothesized characteristic motion can be produced during eating. To test this, data was recorded while a subject consumed five bites of food deliberately attempting to produce the anticipated characteristic motion for each bite. The results of this experiment can be seen in Figure 3.12. Four of the five bites during this experiment match the motion we would expect. However, even when a subject deliberately tried to produce the hypothesized characteristic bite motion, one in five bites failed to meet the criteria. The fourth bite in Figure 3.12 occurring around 18 seconds failed to produce the dual peak effect as the hand motioned toward the mouth.

CHAPTER 4

CONCLUSIONS

In this thesis we have addressed the problem of tracking linear wrist motion using low cost inertial sensors. We have found that the ability of these sensors to track distance deteriorates rapidly within several seconds due to double integration of errors. By detecting periods of rest in the data we find that we can periodically reset the system and thereby create small time windows after rest in which motion can be tracked.

Using the small time windows of tracking data we have analyzed linear motion patterns that occur during the taking of a bite of food. We have found that linear wrist motion is not a good indicator of bite detection. This is mostly due to the high variability of action sequences that occur when taking a bite of food. Another cause for concern is that less than 20% of bites occur within 3 seconds of a rest period indicating that in order to track motion reliably during eating we need to develop a more accurate device.

To increase the device's accuracy we must develop a sensor based on more accurate gyroscopes. MEMS Gyroscope datasheets specify the rate noise density that can be expected. The units of the rate noise density are $\frac{\circ/s}{\sqrt{Hz}}$. The noise level of the gyroscope depends on the sampling frequency. Figure 4.1 shows the effect of the choice of rate noise density and frequency on position tracking errors over time. From this graph it is clear that a lower frequency and a smaller rate noise density will produce more accurate results.

Another important design parameter is the noise that can be expected from the A to D converter. In our case, the Atmega32u4 microcontroller claims ± 2 LSB accuracy. For the LPR530al gyroscope amplified output this means $\pm 1.84^{\circ/s}$ noise level due to the analog to digital converter. The rate noise density for the same gyroscope is $0.035 \frac{\circ/s}{\sqrt{Hz}}$, sampling at a frequency of 110Hz yields a gyroscope noise level of $.367^{\circ/s}$. Therefore, our system is limited by the resolution of the microcontroller's ADC and

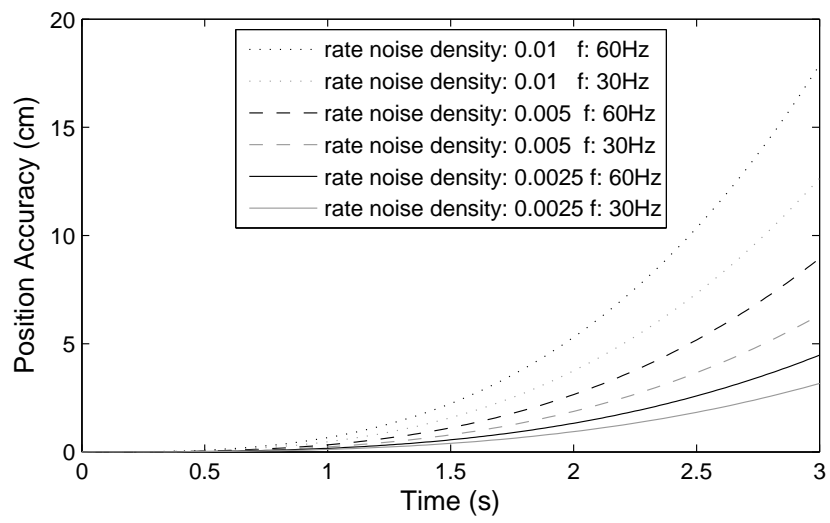


Figure 4.1 The effect of rate noise density and sampling frequency on position accuracy over time

not the sensor we are using. In order to determine the analog to digital converter specifications that will not limit the accuracy of the analog gyroscope Equation 4.1 is used. The noise level is primarily a function of η (the accuracy of the ADC), the resolution of the converter specified in bits, and the sensitivity of the sensor.

$$\text{noiselevel} = \frac{V_{dd} \frac{\eta}{2^{\text{bits}}}}{\text{Sensitivity}} \quad (4.1)$$

Another potential area for device improvement is to calibrate gyroscope sensitivity. Currently, the sensitivity value listed in the datasheet is used to calculate the angular rate. By calibrating this value for each axis of the sensor, errors introduced by the gyroscope may be reduced.

We have made a simplifying assumption in our calculations that there is a single device frame and that the axes of measurement of the gyroscopes and accelerometer are the axes of the device frame. Due to practical issues in construction, the gyroscope axes are translated, and possibly slightly rotated from the accelerometer axes. To account for this anomaly, a misalignment matrix should be calculated as a phase of calibration procedure.

A final way to improve the accuracy of our sensors would be to compute the noise characteristics for the gyroscopes and accelerometer. This analysis is typically performed using an Allan Variance plot [29]. A number of parameters such as quantization error, bias, random walk, and white noise can be read directly off the Allan Variance plot. With a better understanding of the noise in the system, signal processing techniques may be developed to alleviate some of the major system errors.

The work described in this thesis examines accelerations in the coordinate system of the device. An interesting extension to this work would be to examine linear wrist motion during eating in the world coordinate frame. Although without a magnetometer we have no frame of reference to determine the direction of X_e or Y_e , with the aid of the gravity vector we have enough information to compute accelerations along the Z axis of the world frame. We eat in an upright position so that our digestive systems do not have to fight gravity while swallowing food. Viewing accelerations

parallel to gravity would likely reduce the variability between subjects.

Another extension to our work would be to view the acceleration data as a vector rather than a scalar. Throughout this thesis we have analyzed the magnitude of the acceleration that occurs during the taking of a bite of food, ignoring data related to the direction of acceleration. Analyzing all of the available data should yield more insight into the motion being measured.

REFERENCES

- [1] O. Amft, H. Junker, and G. Troster. Detection of eating and drinking arm gestures using inertial body-worn sensors. In *Proceedings - International Symposium on Wearable Computers*, volume (ISWC), pages 160–163, 2005.
- [2] Atmel. *8-bit AVR microcontroller with 16/32K bytes of ISP flash and USB controller*. http://www.atmel.com/dyn/resources/prod_documents/doc7766.pdf.
- [3] W. Bang, W. Chang, K. Kang, E. Choi, A. Potanin, and D. Kim. Self-contained spatial input device for wearable computers. *Seventh IEEE Symposium on Wearable Computers*, (ISWC'03):26, 2003.
- [4] J. Beidler, A. Insogna, N. Cappobianco, Y. Bi, and M. Borja. The pna project. In *Proceedings of the sixth annual CCSC northeastern conference*, volume 16(4), pages 276–84, 2001.
- [5] Dean Camera. Four walled cubicle - lufa(2010). <http://www.fourwalledcubicle.com/LUFA.php>.
- [6] C. Carroll, M. McDowell, and K. Flegal. Division of health and nutrition examination surveys. Technical Report NHCS Brief no 1, National Center for Health Statistics, November 2007.
- [7] C. Champagne, G. Bray, A. Kurtz, J. Monteiro, E. Tucker, and J. Volaufova et. al. Energy intake and energy expenditure: A controlled study comparing dieticians and non-dieticians. *Journal of the American Dietetic Association*, 102:1428–1432, 2002.
- [8] K. Chang, S. Liu, H. Chu, J. Hsu, Y. Jane, C. Chen, and T. Lin nad C. Chen nad P. Huang. The diet-aware dining table: Observing dietary behaviors over a tabletop surface. *Lecture Notes in Computer Science, Pervasive Computing - 4th International Conference*, LCNS 3968:366–382, 2006.
- [9] S. Cho, J. Oh, W. Bang, W. Chang, E. Choi, Y. Jing, J. Cho, and D. Kim. Magicwand: A hand-drawn gesture input device in 3-d space with inertial sensors. *Ninth International Workshop on Frontiers in Handwriting Recognition*, (IWFHR'04):106–111, 2004.
- [10] Yujie Dong. A device for detecting and counting bites of food taken by a person during eating. Master's thesis, Department of Electrical Engineering, Clemson University, 2009.
- [11] K. Glanz, J. Brug, and P. van Assema. Are awareness of dietary food intake and actual fat consumption associated? - a dutch-american comparison. *European Journal of Clinical Nutrition*, 51:542–547, 1997.
- [12] Evelyn Kelly. *Obesity: Health and Medical Issues Today*. Greenwood Publishing Group, 2006.

- [13] L. Lechner, J. Brug, and H. De Vries. Misconceptions of fruit and vegetable consumption: Differences between objective and subjective estimation of intake. *Journal of Nutrition Education*, 29(6):313–320, 1997.
- [14] S. W. Lichtman, K. Pisarska, E. Berman, M. Pestone, H. Dowling, and E. Offenbacher et. al. Discrepancy between self reported and actual caloric intake and exercise in obese subjects. *The New England Journal of Medicine*, 327(27):1894–1898, 1992.
- [15] M. Mahoney. The obese eating style: Bites, beliefs, and behavior modification. *Addictive Behaviors*, 1:47–53, 1975.
- [16] L. Mulheim, D. Allison, S. Heshka, and S. Heymfield. Do unsuccessful dieters intentionally underreport food intake? *International Journal of Eating Disorders*, 24:259–266, 1998.
- [17] World Health Organization. Overweight and obesity, 2008. <http://www.who.int/mediacentre/factsheets/fs311/en/index.html>.
- [18] V. Periwal and C. Chow. Patterns in food intake correlate with body mass index. *Am J Physiol Endocrinol Metab*, 291:E929–E936, 2006.
- [19] William Premerlani and Paul Bizard. Direction cosine matrix imu: Theory, 2009. gentlenav.googlecode.com/files/DCMDraft2.pdf.
- [20] Jenna Scisco. The bite detector: A device for the behavioral treatment of overweight and obesity. Master’s thesis, Department of Psychology, Clemson University, 2009.
- [21] STMicroelectronics. Lis344alh: Mems inertial sensor. <http://www.st.com/stonline/products/literature/ds/14337.pdf>.
- [22] STMicroelectronics. Lpr530al: Mems motion sensor. <http://www.st.com/stonline/products/families/sensors/datasheets/lpr530al.pdf>.
- [23] STMicroelectronics. Lpy530al: Mems motion sensor. <http://www.st.com/stonline/products/families/sensors/datasheets/lpy530al.pdf>.
- [24] A. Subar, V. Kipnis, R. Troiano, D. Midthune, D. Scholler, and S. Bingham et al. Using intake biomarkers to evaluate the extent of dietary misreporting in a large sample of adults. *American Journal of Epidemiology*, 158:1–13, 2003.
- [25] L. Terre, W. Poston, and J. Foreyt. *The Management of Eating Disorders and Obesity: Overview and Future of Obesity Treatment*. Humana Press, Totowa, NJ, 2005.
- [26] David Titterton and John Weston. *Strapdown Inertial Navigation Technology*. Institution of Electrical Engineers, 2nd edition, 2004.
- [27] J. Tooze, A. Subar, F. Thompson, R. Troiano, A. Schatzkin, and V. Kipnis. Predictors of energy and underreporting in a large doubly labeled water study. *American Journal of Clinical Nutrition*, 79:795–894, 2004.

- [28] M. Westerterp-Plantenga. Eating behavior in humans, characterized by cumulative food intake curves-a review. *Neuroscience and Biobehavioral Reviews*, 24:239–248, 2000.
- [29] O. Woodman. An introduction to inertial navigation. Technical Report UCAM-CL-TR-696, University of Cambridge, August 2007.

APPENDIX

